

# EFFECT OF REACTIVE MAGNESIUM OXIDE ON PROPERTIES OF ALKALI ACTIVATED SLAG GEOPOLYMER CEMENT PASTES

<sup>#</sup>H. A. ABDEL-GAWWAD\*, S. ABD EL-ALEEM\*\*

*\*Housing and Building National Research Center, Giza, Egypt*

*\*\*Chemistry Department, Faculty of Science, Fayoum University, Fayoum, Egypt*

<sup>#</sup>E-mail: amdyabdelgawwad@yahoo.com

Submitted March 22, 2014; accepted March 12, 2015

**Keywords:** Reactive magnesium oxide, Calcination temperature, Drying shrinkage, Hydrotalcite like-phases, Magnesium silicate hydrate

*The effect of different proportions and different reactivities of MgO on the drying shrinkage and compressive strength of alkali activated slag pastes (AAS) has been investigated. The slag was activated by 6 wt. % sodium hydroxide and liquid sodium silicate at ratio of 3:3 wt. %. The different reactivities of MgOs were produced from the calcination of hydromagnesite at different temperatures (550, 1000, 1250°C). The results showed that the reactivity of magnesium oxide decreases with increasing the calcination temperature. Also, the drying shrinkage of AAS was reduced by the replacement of slag with MgOs. The highly reactive MgO accelerated the hydration of AAS at early ages. The replacement of slag with 5 % MgO<sub>550</sub> increased one day compressive strength by ~26 % while MgO<sub>1250</sub> had little effect. A significant increase in strength was observed after 7 days in case of replacement of slag with 5 % MgO<sub>1250</sub>. The MgO reacts with slag to form hydrotalcite like-phases (Ht) as detected by XRD, FTIR spectroscopy, TGA/DTG analysis and SEM.*

## INTRODUCTION

Alkali-activated slag (AAS) binders have taken a great interest due to its manufacturing process which has important benefits from the point of view of the lower energy requirements and lower emission of greenhouses gases with respect to the manufacturing of Portland cement. Several studies [1-5] indicate that AAS cements and concretes present high mechanical strength and good performance in chemical attack, frost-thaw cycles and high temperatures. The main application of these binders is in pre-casting and repairing. However, previous researches [6-9] has shown that alkali activated slag mortars and concretes are subject to substantial autogenous and drying shrinkage. This is one of the main drawbacks to the definitive use of AAS as an alternative to traditional Portland cement binders.

There are a number of factors that determine the drying shrinkage of AAS including the type and content of the alkali activators [8, 10-12], properties of the aggregate and the slag [6, 13], as well as curing environment [14-17]. In general, water-glass activated slag has more shrinkage than sodium hydroxide activated slag and the drying shrinkage of AAS increases with increasing dosage of activators as well as slag fineness [18, 12]. In addition, the shrinkage of AAS is very sensitive to the curing environment. It is reported

that although at 70 % RH the drying shrinkage of AAS concrete is similar to that of PC concrete [15], and it is significantly higher at 33 % and 50 % RH [15, 16].

Some authors [19, 20] suggested that the characteristics of hydrated calcium silicate gel and pore size distribution, have a direct effect on the drying shrinkage. According to Kutti [21] two main hydration products are formed as a result of alkali activation of slag, a C-S-H gel similar to the gel formed in Portland cement pastes, although with a lower Ca/Si ratio, and a Si-rich gel with properties similar to silica gel. This latter product contains higher free water content that is eliminated during the drying process, causing substantial shrinkage and therefore microcracking.

In order to reduce the drying shrinkage of AAS concrete, Bakharev et al. [22] investigated the effect of different admixtures on water glass-activated slag concrete. Lower drying shrinkage (at 50 % RH) was observed for the AAS compared to PC concrete prepared with 6 % gypsum and concluded that gypsum reduces both autogenous and drying shrinkage due to the formation of expansive phases such as ettringite (AFt). Specimens with superplasticizer showed the highest drying shrinkage, followed by without admixtures and then with water-reducing admixtures, whilst the specimens containing air-entraining agent exhibited the lowest shrinkage. On the other hand, the compressive

strength results showed that superplasticiser admixture resulted in a 25 % loss of 28 day strength and water reducing (based on lignosulphonates) reduced the early strength up to 14 days, while the air-entraining agent had no negative effect [22]. They concluded that it was not desirable to use superplasticiser in AAS concretes, which is consistent with other findings that some of the conventional admixtures used for PC have detrimental effects in AAS concrete [7, 23]. Palacios and Puertas [24] investigated the effect of polypropylen glycol-based shrinkage-reducing admixture (SRA) on the drying shrinkage of water glass-activated slag mortars. They reported that 1 % and 2 % SRA reduced drying shrinkage by 7 % and 50 % respectively at 50 % RH, while it reduced by 50 % and 85 % respectively at 99 % RH, which was attributed to the change in the pore structure by the admixture and the decrease in the surface tension of the pore water, agreeing well with the suggestions by others [9, 25]. In terms of compressive strength, SRA was found not to cause substantial change under 50 % and 99 % RH.

The use of magnesia, MgO, as a shrinkage reducing mineral additive, dates back to the mid-1970s in the construction of the Baishan concrete arch gravity dam [26], where it proved to be a more efficient and economical measure of controlling the shrinkage of PC than conventional admixtures [27]. The volume compensation during the drying process was due to the chemical reaction between MgO and water forming brucite ( $Mg(OH)_2$ ), which results in 118 % volume increase [28]. The effect of MgO in the AAS systems has recently been investigated, either in terms of its varying natural content in different slag compositions [29], or as an additive [30]. As slags are usually produced at temperatures of 1400-1600°C [31], the MgO naturally present in slags is categorized as dead burned MgO (Pericles) [32]; whereas reactive grade MgO (calcined at temperature lower than 1000°C) or hard burned MgO (calcined at 1000-1400°C) are often chosen for use as additives.

Ben Haha et al. [29] investigated the effect of natural MgO content in different slags on the performance of AAS and revealed that although the main hydration product is still C-S-H gel, MgO reacts with the slag to form hydrotalcite ( $Mg_6Al_2(OH)_{16}CO_3 \cdot 4H_2O$ )-like phases, the content of which increases as the MgO content in the slag increases. They also concluded that since these hydrotalcite like phases are more voluminous than C-S-H, that they result in higher strength, hence the higher the MgO content, the higher the strength. Shrinkage performance was not studied. In the work

by Fei Jin et al. [33] studied the effect of addition of commercial reactive MgO on drying shrinkage and strength of AAS. They are found that MgO with high reactivity accelerated the early hydration of AAS, while MgO with medium reactivity had little effect. The drying shrinkage was significantly reduced by highly reactive MgO but it also generated severe cracking under the dry condition. On the other hand, medium-reactive MgO only showed observable shrinkage-reducing effect after one month, but the cement soundness was improved. The hydration products, analyzed by X-ray diffraction, thermogravimetric analysis and scanning electron microscopy techniques, showed that Mg was mainly incorporated in the hydrotalcite-like phases. It is concluded that the curing conditions and the time of hydrotalcite-like phases formation and their quantity are crucial to the developed strength and shrinkage reduction of MAAS, which are highly dependent on the reactivity and content of reactive MgO.

In this work, the effect of replacement of magnesium oxide with different proportions and different activities on strength and drying shrinkage of AAS was studied. The effect of addition of reactive magnesium oxide on drying shrinkage and strength of AAS was previously studied [30, 33]. However, the effect of replacement of slag by reactive MgO on drying shrinkage and strength of activated slag pastes has not been determined to date, and constitutes the object of the present study.

## EXPERIMENTAL

### Materials

Granulated blast-furnace slag (GBFS) was purchased from Helwan Steel Company. Hydromagnesite was purchased from Arabic Chemical Company. Sodium hydroxide (SH) powder of 99 % purity was obtained from Fisher Scientific Company. Liquid sodium silicate (LSS) with 17 %  $Na_2O$ , 32 %  $SiO_2$  and density of 1.46 was obtained from Arabic Science Company, Egypt.

Table 1 summarizes the chemical composition of granulated blast furnace slag, and hydromagnesite as determined by X-ray Fluorescence (XRF). The mix proportion of MgO-GBFS, alkali activator content and the calcination temperatures of hydromagnesite was presented in Table 2. Figure 1 shows the mineralogical composition of GBFS and hydromagnesite. The figure shows that the granulated slag is mainly amorphous material and hydromagnesite is well crystalline composed of 100 % hydromagnesite without any impurities.

Table 1. Chemical compositions of hydromagnesite and granulated blast-furnace slag (GBFS), wt. %.

Oxide, %	SiO <sub>2</sub>	Al <sub>2</sub> O <sub>3</sub>	Fe <sub>2</sub> O <sub>3</sub>	CaO	MgO	Na <sub>2</sub> O	K <sub>2</sub> O	SO <sub>3</sub>	TiO <sub>2</sub>	P <sub>2</sub> O <sub>5</sub>	L.O.I	Total
Hydromagnesite	0.09	0.08	0.01	0.4	42.95	–	0.18	0.04	-	0.03	56.19	99.94
GBFS	37.81	13.14	0.23	38.70	7.11	1.03	0.19	1.19	0.40	0.17	–	99.97

Table 2. Mixes composition of blended slag cement pastes.

Mix symbol	MgO (wt. %)	GBFS (wt. %)	SH (wt. %)	LSS (wt. %)	W/C ratio	Calcination temperature (°C)
M0	0	100	3	3	0.30	–
M5-550	5	95	3	3	0.30	550
M10-550	10	90	3	3	0.30	550
M15-550	15	85	3	3	0.30	550
M5-1000	5	95	3	3	0.30	1000
M5-1250	5	95	3	3	0.30	1250

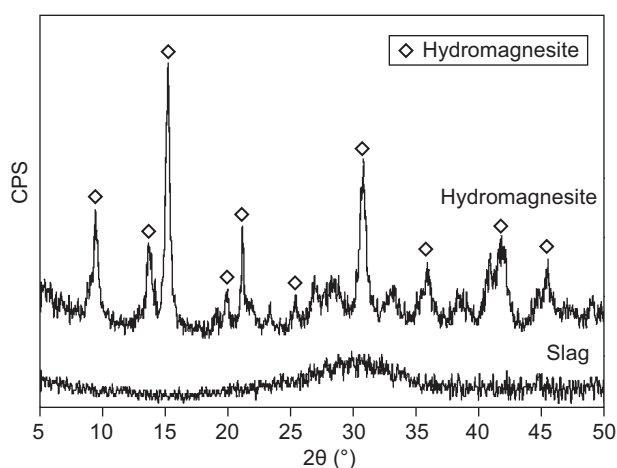


Figure 1. XRD pattern of hydromagnesite and slag samples.

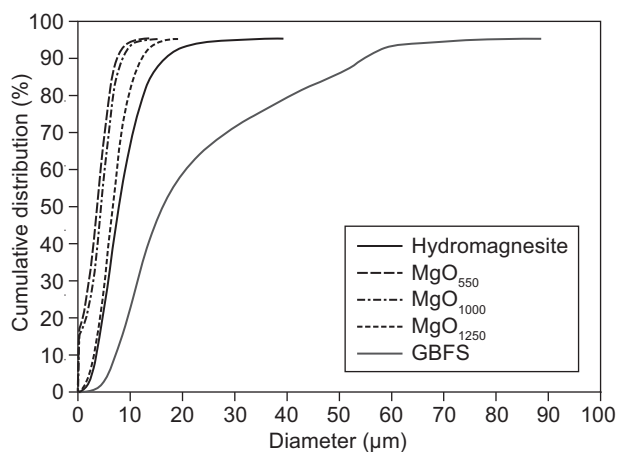
Figure 2. Particle sizes distribution of hydromagnesite and MgO<sub>550</sub>, MgO<sub>1000</sub> and MgO<sub>1250</sub>.

Figure 2 shows the particle size distribution of GBFS, hydromagnesite and MgO calcined at 550, 1000 and 1250°C. It's can be found from particle size distribution that GBFS has about 90 % < 50 μm and 10 % < 7 μm. On the other side, the particle size of HM is mainly lower than 15 μm. The grain size of MgO calcined at 550°C (< 7 μm) is lower than those calcined at 1000°C (< 8 μm) and 1250°C (< 11 μm).

### Calcination of hydromagnesite

Figure 3 presents the DTA thermogram of hydromagnesite. The endotherms located at 68 - 280°C are due to dehydration and dehydroxylation. The carbonate is decomposed at 425 - 486°C [34].

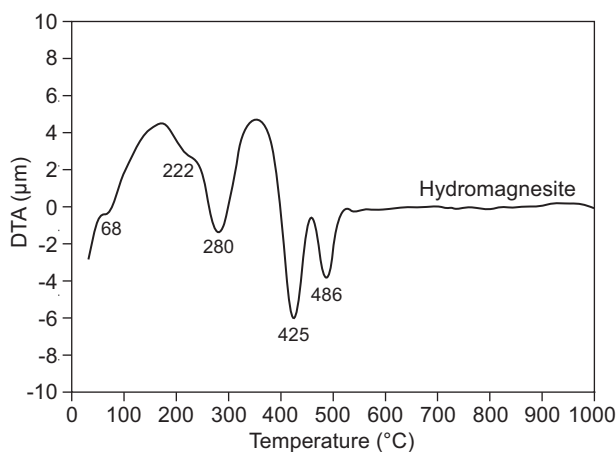
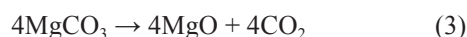
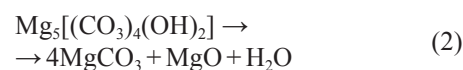
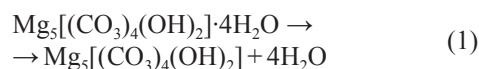


Figure 3. DTA thermogram of hydromagnesite.

The decomposition of hydromagnesite takes place as the follows:



According to the DTA thermogram, the hydromagnesite was calcined at 550, 1000 and 1250°C in order to study the effect of different calcination temperatures on the reactivity and crystallinity of magnesium oxide. The MgO calcined at temperatures 550, 1000 and 1250 namely (MgO<sub>550</sub>, MgO<sub>1000</sub> and MgO<sub>1250</sub>). The calcined MgO was determined by XRD pattern (Figure 4). The XRD diffractograms show that the increase in calcination temperature from 550 up to 1250°C leads to enhance the crystallinity of MgO.

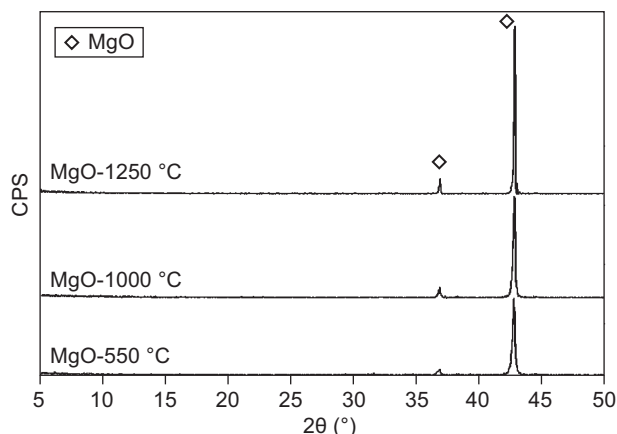


Figure 4. XRD pattern of MgO calcined at 550, 1000 and 1250°C.

The reactivity test was used to measure the time duration required for the neutralization of an acidic solution (0.25 M acetic acid solution) by a certain MgOs ( $\text{MgO}_{550}$ ,  $\text{MgO}_{1000}$  or  $\text{MgO}_{1250}$ ) with mass (5.0 g) and Phenolphthalein was adopted as the pH indicator [35]. The time from adding the MgO to the change of the solution color is recorded as the reactivity and the shorter the time, the more reactive the MgO is. The test was performed in duplicate for each sample and the average value was reported.

#### Alkali activated slag – MgOs pastes preparation

Three MgO-AAS pastes were used in which the reactive MgO, calcined at 550°C, content varied from 5 to 15 % by mass of slag and also, two MgO-AAS paste mixes in which the 5 % MgOs with different activity,  $\text{MgO}_{1000}$  and  $\text{MgO}_{1250}$ , were prepared. All other components were kept constant including water to solid (including the slag, reactive MgO and activators) ratio of 0.30 to ensure good workability. The MgO was first mixed with the slag for 2 min in a bench-top mixer to achieve homogeneity to which the (3:3 wt. %) NaOH: LSS solution (6 wt. % of slag) was then added. The percent of NaOH and LSS was chosen as a result of previous studies [5, 36-38]. After mixing for another 2 min, the mix was cast into the cubic ( $25 \times 25 \times 25$  mm) or prism ( $25 \times 25 \times 285$  mm) moulds in two layers and hand-vibrated to eliminate air voids. The samples were then covered with cling film to avoid moisture loss. After 24 h, the samples were demoulded carefully and the cubes and prisms were transferred into the relative humidity of  $99 \pm 1$  % at  $23 \pm 2$ °C.

#### Methods of investigations

The compressive strength of the specimens were measured after 3, 7, 14, 28, 56 days according to ASTM C109M-12 [39]. Shrinkage was determined as

specified in American standard ASTM C490-07[40]. The length change of activated slag mortar with or without magnesium oxide at any age was calculated as follows:

$$L = (L_x - L_i) / G$$

where  $L$  is the change in length at  $x$  age, %,  $L_x$  is comparator reading of specimen at  $x$  age minus comparator reading of reference bar at  $x$  age.  $L_i$  is initial comparator reading of specimen minus comparator reading of reference bar at that same time.  $G$  is nominal gauge length, 285 mm.

Differential thermal analysis (DTA) and thermogravimetric analysis (TGA) were carried out by heating the sample in nitrogen atmosphere up to 1000°C with a heating rate  $20^\circ\text{C}\cdot\text{min}^{-1}$  using a DT-50 Thermal Analyzer (Schimadzu Co-Kyoto, Japan). The results were compared with DTA standard data. X-ray diffraction analysis was carried out on a Philips PW3050/60 X-ray diffractometer using a scanning range from 5 to 50 with a scanning speed of 1 s/step and resolution of  $0.05$  step $^{-1}$ . Infrared spectra were also recorded from  $4000$   $\text{cm}^{-1}$  to  $400$   $\text{cm}^{-1}$  using Perkin Elmer FTIR Spectrum RX1 Spectrometer. The scanning electron microphotographs were obtained with Inspect S (FEI Company, Holland) equipped with an energy dispersive X-ray analyzer (EDXA).

## RESULTS AND DISCUSSION

#### Determination reactivity degree of MgOs

The reactivity values (as the time increases, the reactivity decreases) of all the MgOs ( $\text{MgO}_{550}$ ,  $\text{MgO}_{1000}$  or  $\text{MgO}_{1250}$ ) powders tested is plotted in Figure 5. It is found that the time required to neutralization of acetic acid by  $\text{MgO}_{550}$ ,  $\text{MgO}_{1000}$  and  $\text{MgO}_{1250}$  are 37 sec., 70 sec. and 163 sec. This is indicated that the  $\text{MgO}_{550}$  was more reactive than that of  $\text{MgO}_{1000}$  and  $\text{MgO}_{1250}$ . This confirms that the reactivity of the calcined MgOs is strongly affected by the thermal conditions of the calcination process [41-43].

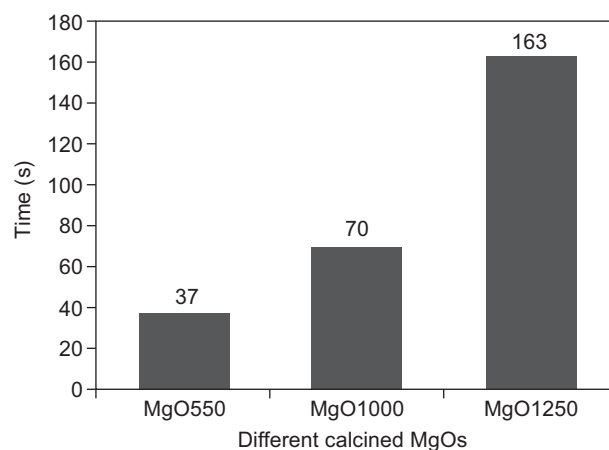


Figure 5. Determination reactivity of MgOs by acetic acid test.

## Compressive strength

Figure 6a shows the effect of  $\text{MgO}_{550}$  contents (5, 10 and 15 %) on the compressive strength of AAS pastes. It is clear from compressive strength results that, there is significant development in the compressive strength at early ages for AAS pastes replaced by 5, 10 and 15 %  $\text{MgO}_{550}$ , respectively. Obviously, a highest increase in strength value ( $\sim 26\%$ ) was achieved for AAS paste replaced by 5 %  $\text{MgO}_{550}$  (M5-550) at 1 day. The reduction in compressive strength was observed when slag replaced by 10 and 15 %  $\text{MgO}_{550}$  (M10-550 and M15-550) but still greater than that of reference sample (M0). The 5 %  $\text{MgO}_{550}$  increase early ages strength up to 7 days while the 10 and 15 %  $\text{MgO}_{550}$  increase early ages strength for only 1 day. The (M5-550) was close and showed nearly the same strength compared to the reference sample after 28 and 90 days. On the other side, the compressive strength values for M10-550, M15-550 was reduced by about 22 %, 30 % at 28 days and 25, 32 % at 90 days compared to reference sample.

Figure 6b shows the effect of  $\text{MgOs}$  ( $\text{MgO}_{550}$ ,  $\text{MgO}_{1000}$  or  $\text{MgO}_{1250}$ ) on strength of AAS pastes. The compressive strength was slightly increased as a result of replacement of slag by 5 %  $\text{MgO}_{1250}$  at early ages (1 and 7 days). The early age's compressive strength of AAS- $\text{MgO}_{550}$  blend was higher than that of the reference sample (M0) and AAS- $\text{MgO}_{1000}$  (M5-1000) and AAS- $\text{MgO}_{1250}$  (M5-1250) blends. A significant increase in strength was observed after 7 days when slag replaced by 5 %  $\text{MgO}_{1250}$ .

Finally, the highly reactive  $\text{MgO}$  accelerate the early age hydration of slag as a result of fast heat release during the dissolution process of  $\text{MgO}$  which accelerate hydration reaction leading to the formation of more hydration products [33]. Martin [44] found that the heat of hydration from highly reactive  $\text{MgO}$  paste was  $> 25$  times higher than that of a less reactive  $\text{MgO}$ . It was measured that the highly reactive  $\text{MgO}$  past's temperature

increased to  $\sim 100^\circ\text{C}$  in 30 min. The replacement of slag by high content of highly reactive  $\text{MgO}$  (10 and 15 %) decreased the compressive strength at later ages. This is due to the fact that  $\text{MgO}$  reacts with broken Si-O or Al-O of AAS to form magnesium silicate hydrate or hydrotalcite like phases (Ht) leading to decrease activated species of  $\text{AlO}_4^-$  and  $\text{SiO}_4^-$  which act as monomers for geopolymer. In addition, the replacement of slag by high content of  $\text{MgO}$  reduces the aluminosilicate content.

## Drying shrinkage

Figure 7 shows the drying shrinkage of AAS and AAS- $\text{MgO}$  pastes up to 90 days. The drying shrinkage of AAS reduced with replacement of slag by 5, 10 and 15 %  $\text{MgO}_{550}$  (M5-550, M10-550 and M15-550) by  $\sim 40$ , 57 and 77 %, respectively, compared to the reference specimens (M0) after 90 days. There is no great difference in the drying shrinkage of M5-1000 and M5-550 especially at later ages. In contrast, the drying shrinkage of low reactive  $\text{MgO}_{1250}$  (M5-1250) paste was nearly close to reference specimen during the first week then showing a final shrinkage (at 90 days) decreased by 15 % than reference specimens. It can be concluded that, the reduction of drying shrinkage of AAS by replacement with  $\text{MgO}$  is referred to expansion by hydration and carbonation of  $\text{MgO}$  [30]. The Ht formed as a result of hydration and carbonation of  $\text{MgO}$  which caused healing for cracks resulted from shrinkage of AAS; the healing property is attributed to lower density of Ht ( $2\text{ g}\cdot\text{cm}^{-3}$ ) compared to tobermorite like CSH ( $2.23\text{ g}\cdot\text{cm}^{-3}$ ), resulting in more effective pore filling and low porosity [29]. The formation rate of Ht increases with the reactivity of  $\text{MgO}$  since the quicker dissolution of  $\text{MgO}$  results in the  $\text{Mg}^{2+}$  being available in the pore water to react with broken Al-O bond within the slag by alkali activation [45].

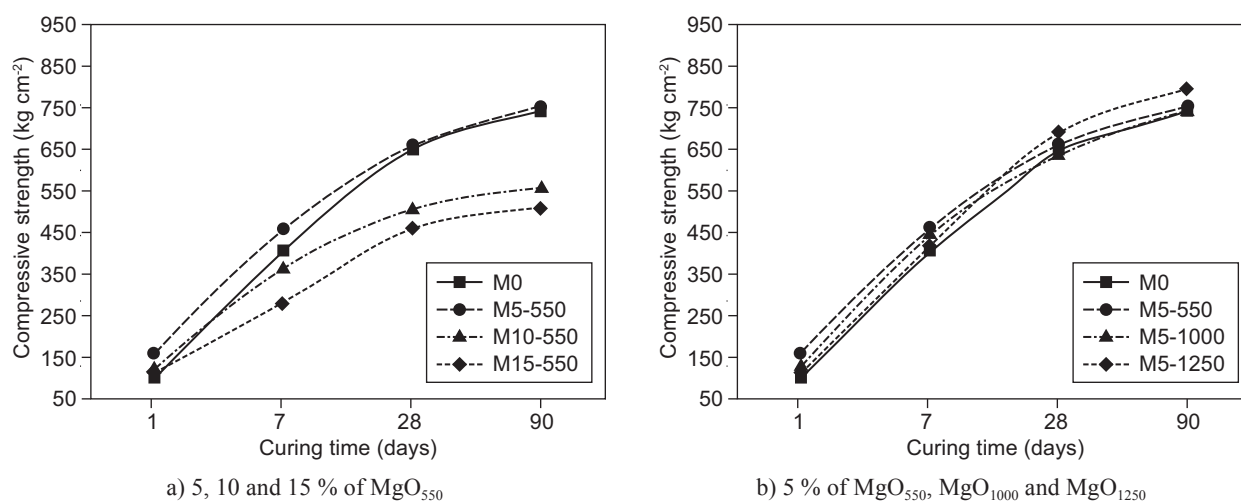


Figure 6. Compressive strength of AAS blended with a) 5, 10 and 15 % of  $\text{MgO}_{550}$  and b) 5 % of  $\text{MgO}_{550}$ ,  $\text{MgO}_{1000}$  and  $\text{MgO}_{1250}$ .

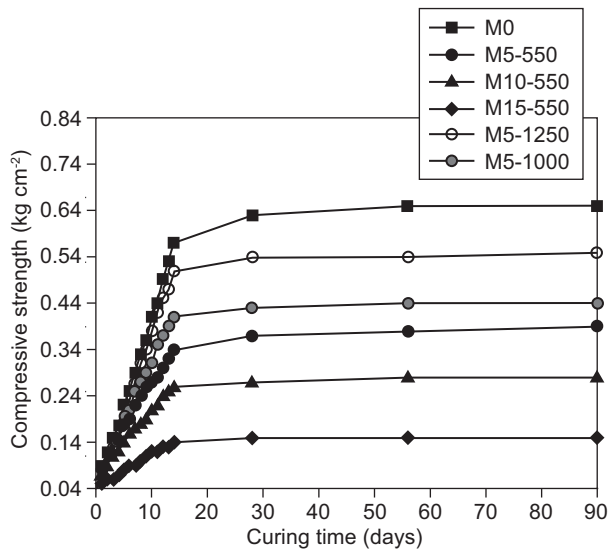


Figure 7. Drying shrinkage of reference specimens and AAS blended with 5, 10 and 15 %  $\text{MgO}_{550}$  as well as blended with 5 % of  $\text{MgO}_{1000}$  and  $\text{MgO}_{1250}$ .

#### Hydration products and microstructure

##### XRD analysis

The major hydration products of AAS detected by XRD are Ht and CSH (Figure 8a,b). The broad and diffuse peak at  $25 - 35^\circ 2\theta$  reflects the short range order of the  $\text{CaO-Al}_2\text{O}_3\text{-MgO-SiO}_2$  glass structure of the slag. Comparing Ht peak intensity at  $2\theta 11.7^\circ$  of M5-550 and M5-1250, it can be found that the intensity of Ht peak of M5-550 is higher than that of M5-1250. This is indicated that the  $\text{MgO}_{550}$  is highly reactive than  $\text{MgO}_{1250}$ . In addition, the higher content of unhydrated MgO (indicated by the higher peak at  $2\theta \sim 42.9^\circ$ ) was detected in pastes with  $\text{MgO}_{1250}$  considering its lower reactivity. Increasing the curing time did not generate new phases, but it increased the crystallinity of C-S-H

as indicated by the sharper peak at around  $2\theta \sim 29.5^\circ$  (Figure 8b) [46]. On the other side, as the contents of  $\text{MgO}_{550}$  increases the Ht peak intensity enhances. Also, the unhydrated MgO peak intensity decreases with the curing time due to formation of more Ht like phase. It should be noted that there was no brucite present in all the pastes regardless of the MgO and its content even at 1 day. According to [47-50], the activation of slag initially consists of a breakdown of the covalent bonds Si-O-Si and Al-O-Si [52]. With the reactive MgO modification, MgO hydrolysed on the surface and either reacts with the broken Si-O or Al-O to form magnesium silicate hydrate (M-S-H) or Ht, hindering the precipitation of brucite. The findings here confirmed early studies that Mg is quickly consumed to form Ht or M-S-H in combination with silica fume or slag [52, 53], although M-S-H is hard to be detected by XRD [54].

##### TG/DTG analysis

The TG/DTG thermograms of pastes cured for 1 and 28 days are seen in Figure (9 a,b) and Figure (10 a,b). From the DTG thermograms, several peaks can be observed. For temperatures up to  $250^\circ\text{C}$ , the weight loss was attributed to the dehydration of C-S-H and M-S-H [53, 55, 56]. The temperature range of  $250 - 500^\circ\text{C}$  denotes the decomposition of Ht. The small peak at around  $520 - 570^\circ\text{C}$  was attributed to the loss of coordinated water in M-S-H [57]. The temperature range of  $600 - 900^\circ\text{C}$  is the decomposition range of various carbonate-containing phases including Ht [58], magnesium carbonate [59], and calcium carbonate [60], originating from the raw material and the carbonation due to exposure to the air. Generally, all the weight losses increased with the increase of MgO content and the curing time, which is attributed to the higher hydration degree thus more hydration products formed. The weight loss of M15-550 (10.34 and 12.03 %) is greater than that of

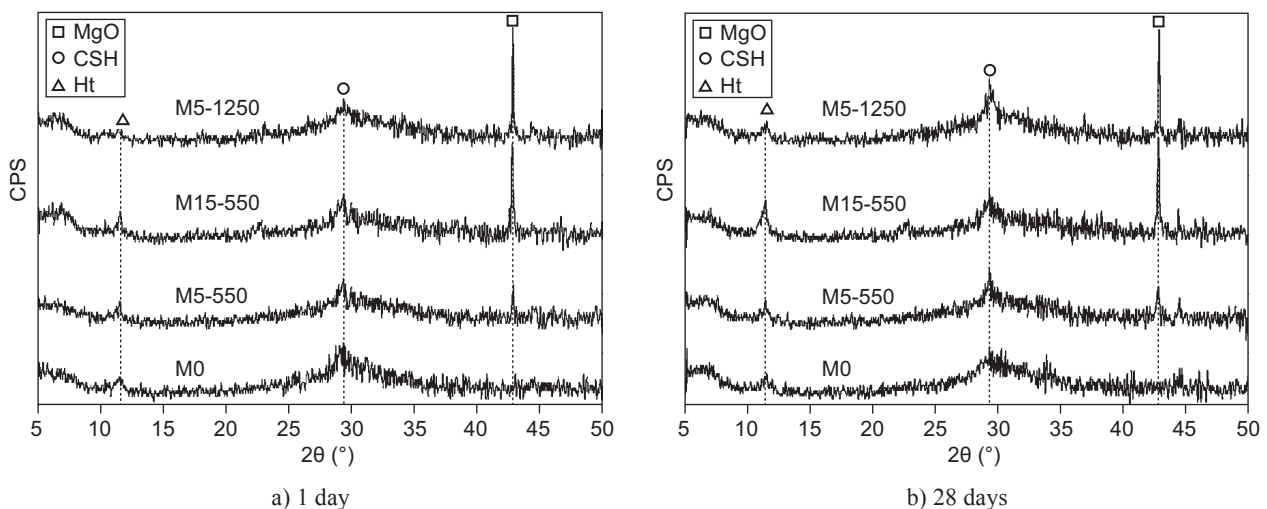


Figure 8. XRD diffractograms of reference specimens and AAS-MgO blends after a) 1 day and b) 28 days.

M5-550 (8.31 and 9.46 %) and reference specimens (7.71 and 8.89 %) for 1 day and 28 days. This is due to the fact that as MgO content increases the *Ht* and *MSH* increase as indicated in DTG curves. On the other side, the weight loss of M5-1250 specimens (7.03 %) is lower than that of M5-550 (8.31 %) at 1 day; this indicated that the low reactivity of  $MgO_{1250}$  which leads to the formation of low amount of *Ht* and *MSH*. The weight loss of M5-1250 (10.36 %) is greater than that of M0 (8.89 %) and M5-550 (9.46 %) at 28 day. In conclusion, the highly reactive  $MgO_{550}$  accelerated the hydration of slag remarkably at 1 day while the  $MgO_{1250}$  had little effect. At 28 day, both MgO increase the rate of hydration of slag.

FTIR analysis

Figure (11 a,b) shows the FTIR spectra of MgO-AAS specimens at 1 day and 28 days. The results indicate that there were different absorption bands. The absorption band at 464 - 492  $cm^{-1}$  is due to O-Si-O bonds

bending vibration. Additionally, relatively well-resolved band at 658 - 716  $cm^{-1}$  has appeared which is associated to the symmetric stretching vibrations of Si-O-Al bridges. The absorption bands located at 952-974  $cm^{-1}$  are due to Si (Al)-O asymmetric stretching vibrations. The absorption band located at 1640 - 1649  $cm^{-1}$  is due to bending H-O-H vibration and the absorption band at 3444 - 3469  $cm^{-1}$  is due to stretching of O-H groups. The absorption bands located at 1382 - 1465  $cm^{-1}$  are due to carbonate group of calcium carbonate, magnesium carbonate or *Ht*. It can be noted that the intensity of absorption bands characteristic for bending H-O-H vibration and stretching of O-H groups increases with increasing of curing time for all mixes. This is attributed to increase of hydration products with curing time. Obviously, the intensity of absorption bands related to symmetric stretching vibrations of Si-O-Al bridges and asymmetric stretching vibrations of Si (Al)-O decrease with increasing the amount of  $MgO_{550}$  for 1 and 28 days of curing. This proves the reaction between activated species (Al-O and Si-O) and MgO which leads to the

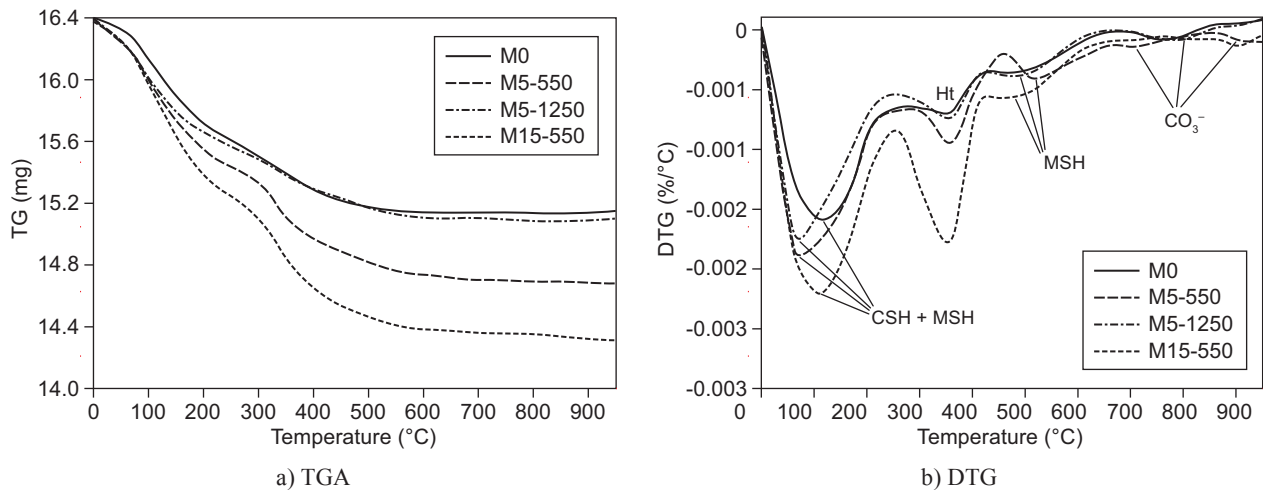


Figure 9. TGA (a) and DTG (b) of AAS and AAS-MgO blends after 1 days.

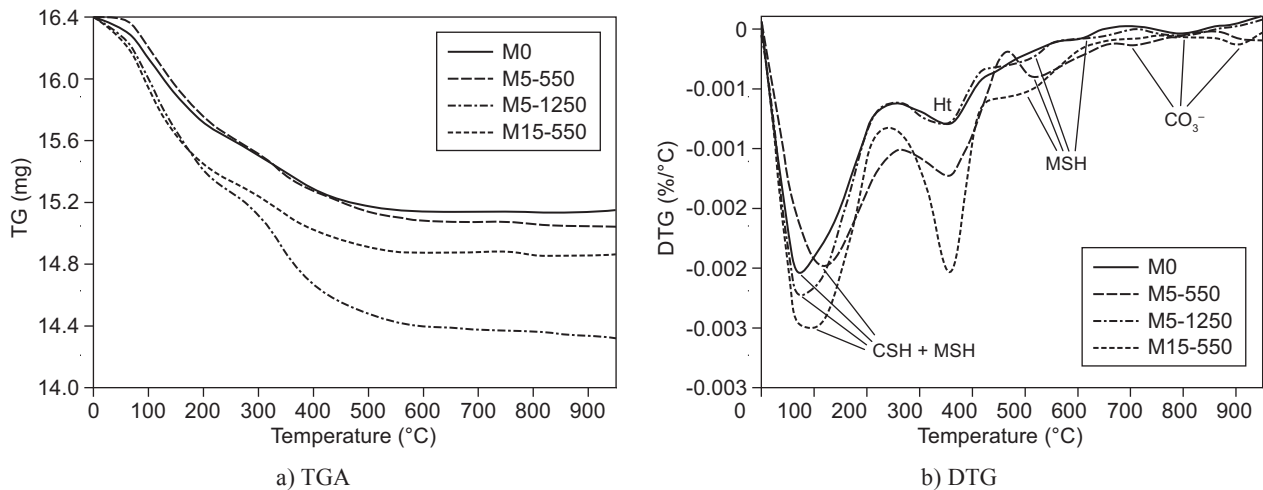


Figure 10. TGA (a) and DTG (b) of AAS and AAS-MgO blends after 28 days.

formation of MSH and *Ht*. This can be observed from the intensity of the bands related to bending H–O–H vibration and stretching of O–H groups which increases with increasing of MgO<sub>550</sub> content. In addition, the replacement of slag on the expense of aluminosilicate content leads to decrease the intensity of aluminosilicate bands. In contrast, the intensity of bands related to symmetric stretching vibrations of Si–O–Al bridges and asymmetric stretching vibrations of Si (Al)–O of AAS-MgO<sub>1250</sub> blend (M5-1250) are higher than those of AAS-MgO<sub>550</sub> blend (M5-550) especially after 28 days. Also, the high full width at half maximum (FWHM), the low FWHM the more crystalline and ordered structure, which especially noticeable in the case of the most intense band at 958 cm<sup>-1</sup> of M5-1250 is lower than that of M5-550 and reference specimens (M0). This is attributed to the high crystalline (low reactive) MgO<sub>1250</sub> acts as nucleation centers which accelerate the rate of crystal geopolymer formation. This indicated that the increase of strength of M5-1250 after 28 days [61].

Figures 12 show the SEM micrograph of MgO-AAS pastes at 1 and 28 days. The microstructure of M5-550, M10-550 and M15-550 is highly compacted and more dens than that of the reference sample (M0) and M5-1250 at early age (1 day). This is mainly due to two reasons. Firstly, the replacement of slag by highly reactive MgO<sub>550</sub> caused the acceleration the early age hydration of slag which leads to the formation of a dens CSH gel and therefore the highly chemically combined water was generated as shown in TG/DTG (Figures 9a,b). The gels have occupied the spaces that were initially filled with water and generated a more compact microstructure further lead to increased strength as presented in Figure 6a. Secondly, the MgO reacts with broken Al–O and Si–O forming *Ht* and M–S–H, The *Ht* was clearly observed in case of M5-550 and M15-550. The *Ht* is more voluminous than C–S–H and therefore occupies more spaces which leads to generate dens and

compact microstructure. After 28 days, all pastes formed dense microstructure with cracks which observed in case of reference specimens (M0) and M5-1250.

## CONCLUSION

The main findings of this study can be summarized as follows:

- The crystallinity of MgO increases with increasing the calcination temperature, therefore the reactivity of MgO decreases.
- The highly reactive MgO<sub>550</sub> accelerated hydration and consequent increases the early compressive strength of AAS pastes while the low reactive MgO<sub>1250</sub> had little effect.
- The acceleration of hydration of AAS-MgO at early ages is ascribed to the heat released during the hydration of MgO.
- The replacement of slag by 5 % low reactive MgO<sub>1250</sub> significantly improved the compressive strength at later age of curing. This is attributed to the high crystalline (low reactive) MgO<sub>1250</sub> which acts as nucleation centers and accelerate the rate of crystal geopolymer formation .
- The replacement of slag by 5, 10 and 15 % MgO<sub>550</sub> reduced the drying shrinkage of AAS by ~ 40 %, 57 % and 77 % after 90 days. Also, The drying shrinkage of M5-1000 showed nearly the same compared to M5-550 especially at later ages. In contrast, the drying shrinkage of low reactive MgO<sub>1250</sub> (M5-1250) paste was close to reference specimens during the first week then showing a final shrinkage (at 90 day) decreased by 15 % than the reference specimens.
- The MgO reacts with slag to form *Ht* like phases which is responsible for the reduction of drying shrinkage of AAS as indicated by XRD, TG/DTG, FTIR and SEM analyses.

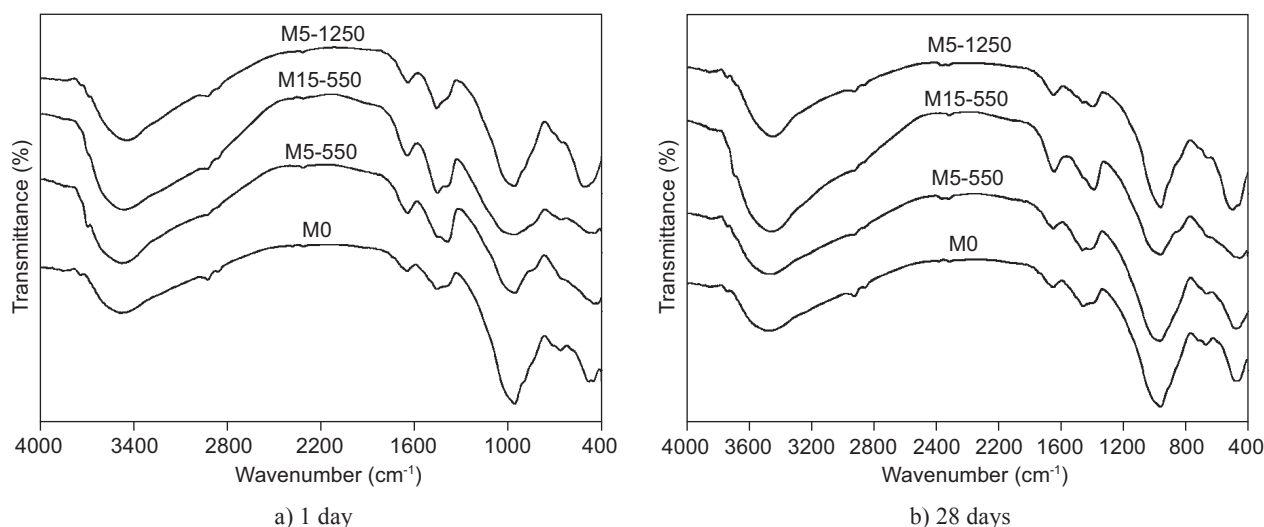
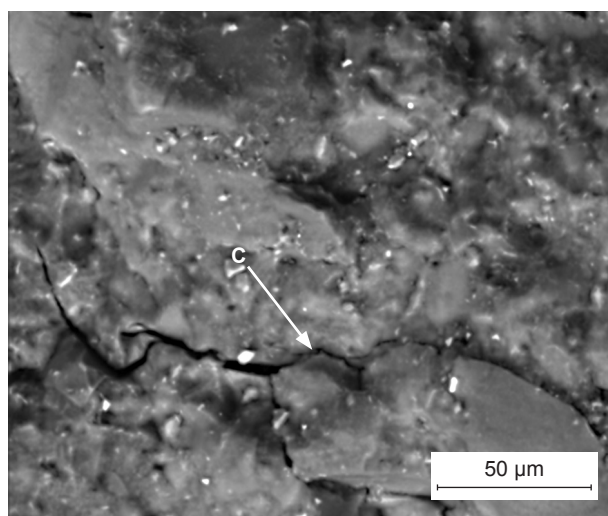
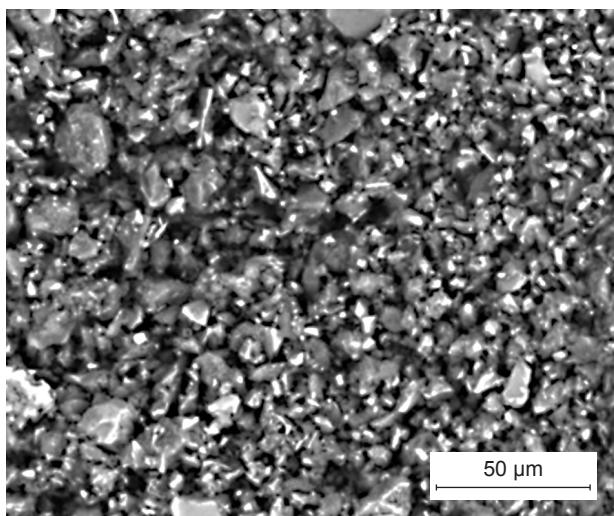
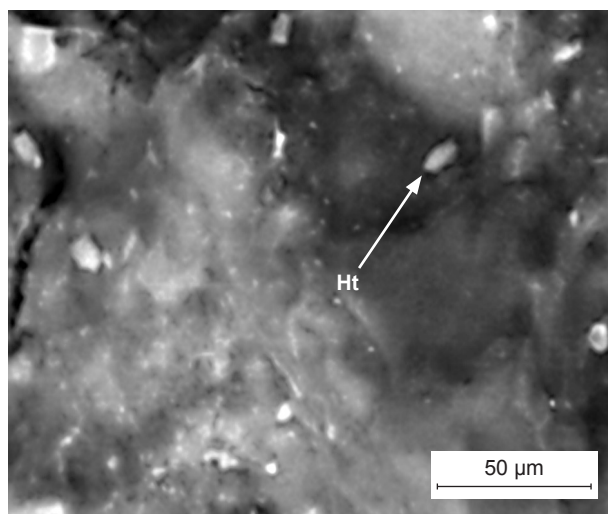
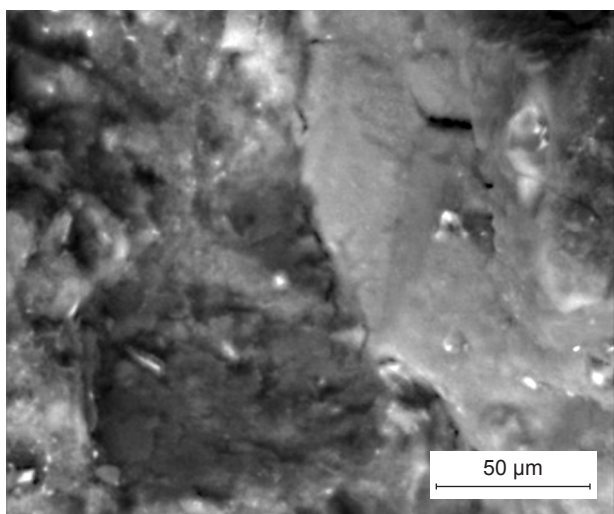


Figure 11. FTIR spectra of AAS and ASS-MgO blends after a) 1 day and b) 28 days.

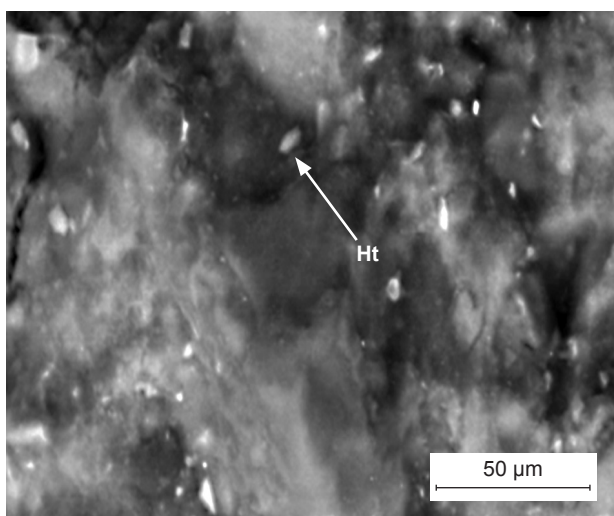
M0



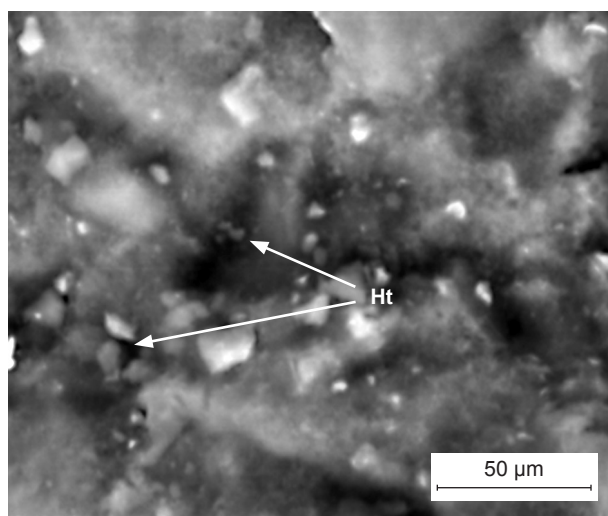
M5-550



M10-550



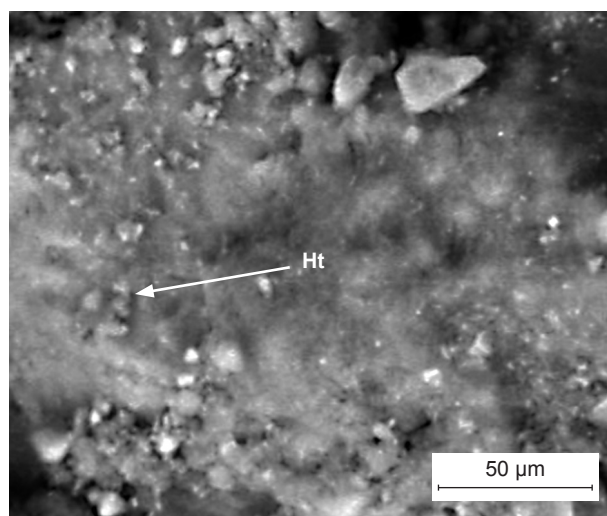
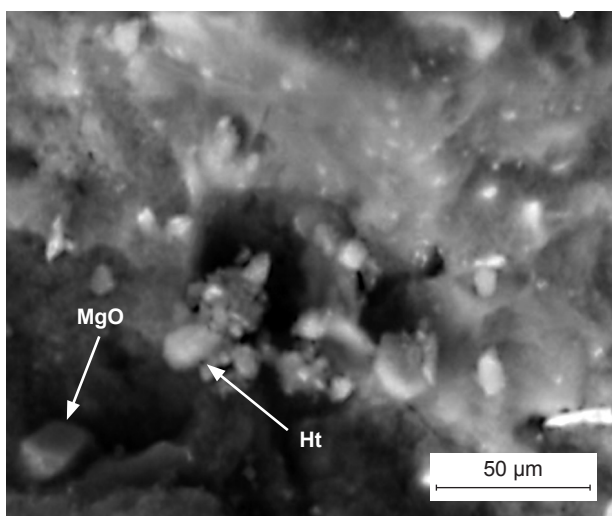
a) 1 day



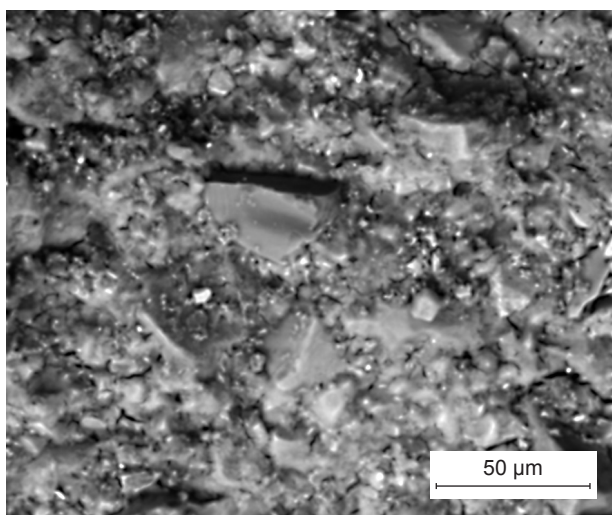
b) 28 days

Figure 12. SEM of AAS and AAS-MgO after a) 1 day and b) 28 days. (continue on next page)

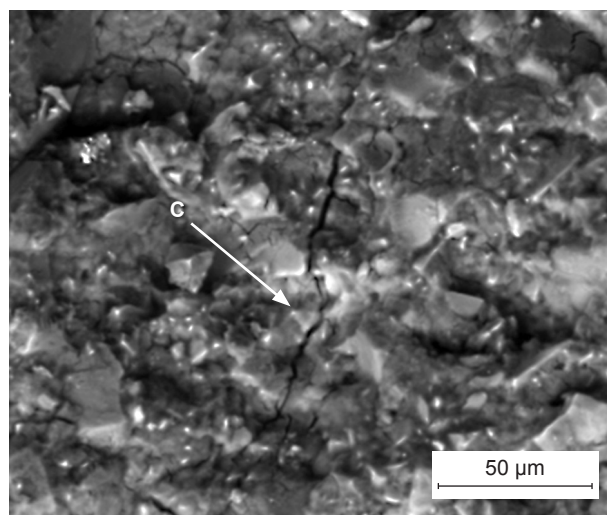
M15-550



M5-1250



a) 1 day



b) 28 days

Figure 12. SEM of AAS and AAS-MgO after a) 1 day and b) 28 days.

## REFERENCES

1. Fernández-Jiménez A., Puertas F., Palomo J. G.: *Cem. Concr. Res.* 29, 593 (1999).
2. Puertas F., de Gutierrez R., Fernández-Jiménez A., Delvasto S., Maldonado J.: *Mater. Constr.* 52, 55 (2002).
3. Cahit Bilim, Okan Karahan, Cengiz Duran Atis, Serhan Ilkentapar: *Mat. Desig.* 44, 540 (2013).
4. Chi-Che Hung, Jiang-Jhy Chang: *Marine Sci. Tech.* 21, 229 (2013).
5. El-Didamony H., Amer A.A., Abd El-Aziz H.: *Ceram. Inter.* 38, 3773 (2012).
6. Cincotto M.A., Melo A.A., Repette W.L. in: *Proceedings of the 11<sup>th</sup> International Congress on the Chemistry of Cement*, Ed. Grieve G., Owens G., p. 1878–88, Durban 2003.
7. Collins F., Sanjayan J.G.: *Cem. Concr. Res.* 29, 607 (1999).
8. Bakharev T., Sanjayan J.G., Cheng Y.B.: *Cem. Concr. Res.* 29, 113 (1999).
9. Collins F., Sanjayan J.G.: *Cem. Concr. Res.* 29, 455 (1999).
10. Shi. C: *Cem. Concr. Res.* 26, 1789 (1996).
11. Shi C., Day R.L.: *Cem. Concr. Res.* 26, 439 (1996).
12. Krizan D., Zivanovic B.: *Cem. Concr. Res.* 32, 1181 (2002).
13. Andersson R., Gram H.E., Malolepszy J., Deja J.: *Alkali-activated slag*. Report No. 1988:1, 1988.
14. Hikkinen T.: *Cem. Concr. Res.* 23, 407 (1993).
15. Kutti T., Berntsson L., Chandra S.: *Proc. 4th CANMET/ACI Int Conf on Fly Ash, Slag, and Natural Pozzolans in Concrete*, Istanbul, Turkey, p. 615–25, 1992.
16. Douglas E., Bilodeau A., Malhotra V.M.: *ACI Mater. J.* 89, 509 (1992).
17. Li Y., Sun Y.: *Cem. Concr. Res.* 30, 963 (2000).
18. Melo Neto A.A., Cincotto M.A., Repette W.: *Cem. Concr. Res.* 38, 565 (2008).
19. Wittmann F.H. in: *Creep and shrinkage in concrete structures*. Eds. Bazant Z.P., Witmann F.H., p. 129, Wiley, Chichester 1982.
20. Young J.F. in: *Mathematical modelling of creep and shrinkage of concrete*. Ed. Bazant Z.P., p. 63, Wiley, Chichester 1988.

21. Kutti T. in: Proc. Int. Congr. On the Chemistry of Cement, New Delhi. p. 468, 1992.
22. Bakharev T., Sanjayan J.G., Cheng Y.B.: Cem. Concr. Res. 30, 1367 (2000).
23. Rashad A.M.: Constr. Build. Mater. 47, 29 (2013).
24. Palacios M., Puertas F.: Cem. Concr. Res. 37, 691 (2007).
25. Collins F., Sanjayan J.G.: Cem. Concr. Res. 30, 1401 (2000).
26. Lou Z., Ye Q., Chen H., Wang Y., Shen J.: J. Chin. Ceram. Soc. 26, 430 (1998).
27. Gao P., Wu S., Lin P., Wu Z., Tang M.: Chin. J. Inorg. Chem. 23, 1063 (2007).
28. Holt E.E.: *Early age autogenous shrinkage of concrete*. Technical Research Center of Finland, p. 446, 2001.
29. Ben Haha M., Lothenbach B., Le Saout G., Winnefeld F.: Cem. Concr. Res. 41, 955 (2011).
30. Shen W., Wang Y., Zhang T., Zhou M., Li J., Cui X.: J. Wuhan Univ. Technol. Mater. Sci. Ed. 26, 121 (2011).
31. Shi C., Krivenko P.V., Roy D.M.: *Alkali-activated cements and concretes*. Taylor & Francis; 2006.
32. Shand M.A.: *The chemistry and technology of magnesia*. Hoboken, New Jersey: John Wiley & Sons, Ltd., 2006.
33. Fei Jin, Kai Gu, Abir Al-Tabbaa: Constr. Build. Mater. 51, 395 (2014).
34. Vágvölgyi F. V., Frost Ray L., Hales M., Locke A., Kristóf J., Horváth E.: J. Therm. Anal. Calorim. 92, 893 (2008).
35. Shand M.A.: *The Chemistry and Technology of Magnesia*. John Wiley & Sons, Ltd., Hoboken, New Jersey, 2006.
36. El Didamony H., Assal H.H., El Sökkary T.M., Gawwad H.A.: HBRC J. 6, 47 (2010).
37. El-Didamony H., Amer A.A., El-Sökkary T.M., Abd-El-Aziz H.: Ceram. Intern. 39, 171 (2013).
38. El Didamony H, Assal H.H., El Sökkary T.M., Abdel Gawwad H.A.: HBRC J. 8, 170 (2012).
39. ASTM C109M, *Standard test method for compressive strength of hydraulic cement mortars*. 2012.
40. ASTM C490-07. *Standard Practice for Use of Apparatus for the determination of Length Change of Hardened Cement Paste, Mortar, and Concrete*. 2007.
41. Birchal V.S., Rocha S.D., Ciminelli V.S.: Minerals engineering 13, 1629 (2000).
42. Mo L, Deng M, Tang M.. Effects of calcination condition on expansion property of MgO-type expansive agent used in cement-based materials.” Cement and Concrete Research2010; 40(3):437–46.
43. Sun W.H., Cui C., Zhang H.H., Cui K.H.: J. Wuhan University of Technology 13, 21 (1991).
44. Liska M.: *Properties and applications of reactive magnesia cements in porous blocks*. PhD. thesis. University of Cambridge, 2009.
45. Jin F, Abdollahzadeh A., Al-Tabbaa A. In: Proceedings of 3rd international conference on sustainable construction materials and technologies. Kyoto, Japan, 2013.
46. Bernal S.A., Provis J.L., Rose V., Gutiérrez R.M.: J. Am. Ceram. Soc. 96, 1951 (2013).
47. Pacheco-Torgal F., Castro-Gomes J., Jalali S.: Constr. Build. Mater. 22, 1315 (2008).
48. Yip C.K., Lukey G.C., van Deventer J.S.J.: Cem. Concr. Res. 3, 1688 (2005).
49. Provis J., Lukey G., van Deventer J.: Chem. Mater. 17, 3075 (2005).
50. Provis J.L., Duxson P., Van Deventer J.S.J., Lukey G.C.: Chem. Eng. Res. Des. 83, 853 (2005).
51. Li C., Sun H., Li L.: Cem. Concr. Res. 40, 1341 (2010).
52. Zhang T., Cheeseman C.R., Vandeperre L.J.: Cem. Concr. Res. 41, 439 (2011).
53. Jin F, Al-Tabbaa A.: Thermochim. Acta. 566, 162 (2013).
54. Brew D.R.M., Glasser F.P.: Cem. Concr. Res. 35, 85 (2005).
55. Dweck J., Buchler P.M., Coelho A.C.V., Cartledge F.K.: Thermochim Acta 346, 105 (2000).
56. Alarconruiz L., Platret G., Massieu E., Ehlacher A.: Cem. Concr. Res. 35, 609 (2005).
57. Tartaglione G., Tabuani D., Camino G.: Microporous Mesoporous Mater. 107, 161 (2008).
58. Parashar P., Sharma V., Agarwal D.D., Richhariya N.: Mater. Lett. 74, 93 (2012).
59. Demir F., Donmez B., Okur H., Sevim F.: Chem. Eng. Res. Des. 81, 618 (2003).
60. Dweck J., Ferreira da Silva P., Büchler P., Cartledge F.: J. Therm. Anal. Calorim. 69, 179 (2002).
61. Duxson P., Provis J.L., van Deventer J.S.J.: *Geopolymers: Structures, processing, properties and industrial applications*. Woodhead Publishing, Abingdon UK, 2009.